

TOPOGRAPHY OF THE FOVEAL CONE MOSAIC IN THE LIVING HUMAN EYE

DAVID R. WILLIAMS

Center for Visual Science, University of Rochester, Rochester, NY 14627, U.S.A.

(Received 21 April 1987; in revised form 31 July 1987)

Abstract—Interference fringes whose spatial frequency exceeds the resolution limit form visible moiré patterns with the foveal cone mosaic. This paper describes a model of foveal cone sampling that shows how these moiré patterns depend on the spatial frequency and orientation of an interference fringe imaged on a triangular lattice of cones. The model is tested with two psychophysical experiments. The first experiment shows that the behavior of the moiré patterns is quantitatively consistent with anatomical estimates of cone spacing across the human fovea. These patterns provide a psychophysical method for measuring cone spacing within 1.75 deg of the foveal center. In some observers, cone spacing is larger in a horizontal direction than in a vertical direction at any particular location within the fovea. The second experiment shows that the behavior of the moiré patterns is consistent with the triangular packing of foveal cones observed anatomically, and allows the orientation of the cone mosaic to be determined at the foveal center. These observations demonstrate the rich information that methods based on aliasing can provide about the topography of foveal cones in the living human eye.

Cone spacing Fovea Laser interferometry Mosaic Aliasing Sampling Spatial vision
Resolution Acuity Human

INTRODUCTION

Despite the importance of the fovea for human vision, there exists surprisingly little quantitative information about its topography. Österberg's classic study (1935) of the distribution of cones across the human retina is based on a detailed study of a single human eye. A recent study by Curcio *et al.* (1987) provides anatomical estimates of human cone spacing in an additional four eyes. There have also been recent estimates of cone spacing in the monkey

(Perry and Cowey, 1985; de Monasterio *et al.*, 1985; Hirsch and Miller, 1987). However, the foveal cone mosaic is extremely fragile, even in the hands of the most skilled anatomist, and it is difficult to be certain that measurements of the mosaic have not been distorted by shrinkage and other forms of histological artifact. This paper describes a noninvasive, psychophysical technique that allows the topography of the foveal mosaic to be mapped in the living eye.

Byram (1944) discovered that interference fringes could be detected in the fovea even when they were much finer than the resolution limit of about 60 c/deg.* These high frequency interference fringes have a wavy, shimmering appearance that Byram suggested was a moiré pattern formed with the cone mosaic. The moiré patterns could be seen at spatial frequencies as high as 150 c/deg. Williams (1985a) extended these observations with an improved laser interferometer, and presented the first direct evidence that the entoptic "zebra stripes" seen by observers viewing fine fringes were indeed caused by cone aliasing. The appearance of the zebra stripes at the foveal center was quantitatively consistent with the moiré patterns predicted from anatomical estimates of foveal cone spacing. Aliasing has also been observed

*Helmholtz (1962) noted that at spatial frequencies of 46–50 c/deg and above, a fine pattern of parallel wires viewed in the fovea appears distorted. He attributed this effect to the cone mosaic. The author (Williams, 1985a) rejected Helmholtz's suggestion because this range of frequencies lies below the Nyquist frequency at the foveal center of about 56 c/deg on average. I also incorrectly reported the range of frequencies over which Helmholtz observed the phenomenon. The spatial frequency range actually reported by Helmholtz is above the cone Nyquist frequency for retinal eccentricities beyond about a half degree from the foveal center. It is possible that Helmholtz was indeed viewing the first hints of aliasing by the foveal or parafoveal cone mosaic, despite the fact that he was viewing gratings in incoherent light. The author has observed similar effects produced by the high spatial frequency raster of television screens displaying a uniform field.

under conditions that isolate the blue-sensitive mechanism (Williams and Collier, 1983a; Williams *et al.*, 1983b) and in the extrafoveal retina (Williams, 1985a; Coletta and Williams, 1987; Williams and Coletta, 1987; Thibos *et al.*, 1987; Smith and Cass, 1987).

The present paper develops a theoretical framework for deducing the topography of the foveal mosaic from the entoptic moiré patterns produced by aliasing. It confirms the anatomical evidence for a quasi-regular packing arrangement of foveal cones, and presents measurements of cone spacing across the living human fovea.

I. MODEL OF FOVEAL ALIASING

To use aliasing to explore foveal topography, we must first develop a theoretical model that shows how the observed moiré patterns should depend on the properties of both the stimulus and the mosaic. The retinal image is effectively two-dimensional, so that the sampling theory developed originally for one-dimensional signals must be extended to two dimensions (see Peterson and Middleton, 1962; Mersereau, 1979; and Fales *et al.*, 1984 for treatments of two-dimensional sampling theory). The model is developed in the spatial frequency domain since intuitions about the behavior of moiré patterns are more easily visualized in frequency than in space. The components of the model are described qualitatively here; a more rigorous description can be found in the Appendix.

Interference fringes

The stimulus is an interference fringe, centered on the fovea, whose intensity is a cosine function of position along one retinal meridian, as shown in Fig. 1(A). The fringe has a period, $1/f$, and an orientation, θ . Figure 1(B) shows the amplitude spectrum of the stimulus in the spatial frequency plane. It consists of three delta

functions: one at the origin, the zero-order delta function, and two that are symmetrically positioned with respect to the origin. I will refer to these latter two as the *first-order delta functions* of the fringe spectrum. The distance from the origin of the first-order delta functions specifies the fringe spatial frequency, f , and their angular position relative to the positive v axis specifies the fringe orientation, θ .

Optics of the eye

For present purposes, the eye's optics are assumed to have no effect on interference fringes for spatial frequencies out to the highest passed by the pupil. The pupil cut-off frequency, expressed in cycles/deg, is $\pi p/180\lambda$, where p is the diameter of the pupil and λ the wavelength of light (Goodman, 1968). Thus for a dilated 8 mm pupil and $\lambda = 632.8$ nm, the highest spatial frequency that can be imaged on the retina is 221 c/deg. This cut-off is well above the highest frequency at which aliasing has been identified in the fovea (about 150–160 c/deg, Williams, 1985a), and is omitted in the model.

The photoreceptor mosaic

The interference fringe is imaged on an idealized cone mosaic in the model. The mosaic is an array of circular elements whose terms form a triangular lattice,* as shown in Fig. 1(C). To simplify the analysis, the mosaic is assumed to be perfectly regular.

Each cone has an aperture of finite diameter whose effect on an interference fringe is to reduce contrast with increasing spatial frequency. The low pass filtering performed by the cone aperture is one of the factors limiting the highest spatial frequencies at which aliasing can be seen (Miller and Bernard, 1983; Williams, 1985a, b). We ignore the effect of the cone aperture for the time being, since it has been shown (see the Appendix) that the demodulation it produces is not severe enough to obliterate the moiré effects of interest here. For present purposes, it is convenient to strip away the cone aperture from the mosaic and to consider only the locations of the centers of cones in the array. This lattice, depicted with solid dots in Fig. 1(C), is critical for understanding the sampling consequences of the mosaic. Each cone center is surrounded by six equidistant neighbors with angular separations of 60 deg between neighbors. Note that cones arranged in this way have three cardinal axes, corresponding to parallel rows of cones that run

*The terms "hexagonal" and "triangular" are both used to describe this lattice (e.g. Ahuja and Schachter, 1983; Shapiro *et al.*, 1985). If foveal cones were truly hexagonal in crosssection with no gaps between them, there would be no ambiguity in describing the mosaic as a "hexagonal tessellation" (Coxeter, 1969). However, the analysis of the sampling properties of the cone mosaic rests on the lattice of points corresponding to cone centers. This lattice is specified by the vertices of a tessellation of triangles rather than hexagons. This motivates the use of the term "triangular" to describe the corresponding lattice.

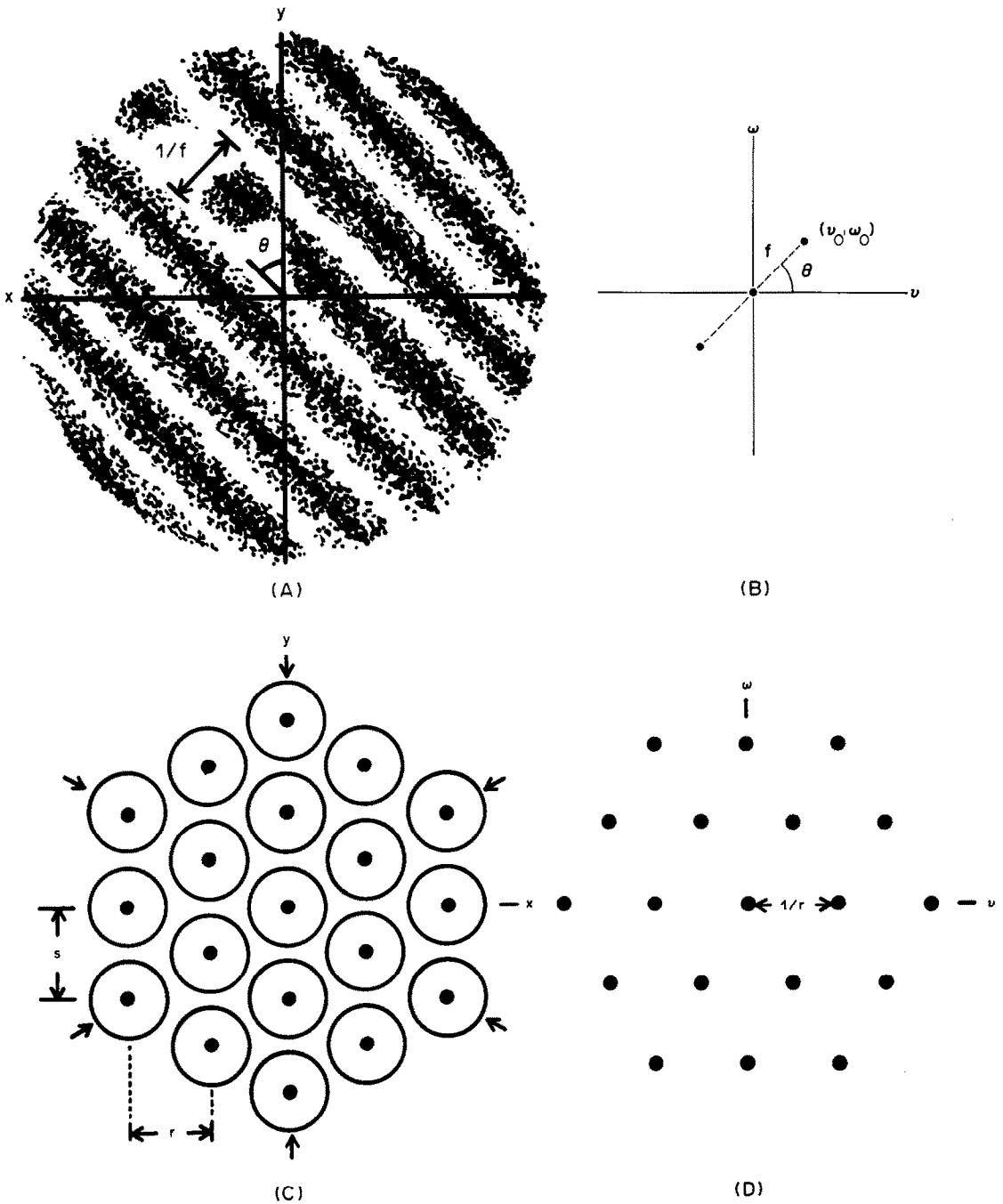


Fig. 1. (A) Sinusoidal interference fringe with spatial period, $1/f$, and orientation, θ . (B) Fourier transform of interference fringe depicted in the 2-D spatial frequency plane. The transform consists of three delta functions: a zero-order component at the origin and two first order delta functions at coordinates (v_0, ω_0) and $(-v_0, -\omega_0)$. The spatial frequency, f , of the fringe is specified by the distance of the first order delta functions from the origin, indicated by the dotted line. The orientation of the fringe is specified by θ . (C) Section of the regular mosaic of cones employed to model foveal aliasing. The large circles represent the apertures of individual cones, whose centers are indicated by black dots. The array of cone centers forms a perfect triangular lattice with center to center spacing, s , and row spacing, r . The three cardinal axes of the mosaic are defined by the orientations of rows of cones, and are indicated by the arrows around the perimeter of the mosaic. (D) Fourier transform of the lattice of cone centers, which is also a triangular lattice. The six delta functions surrounding the delta function at the origin are the *first-order delta functions* of the mosaic spectrum. The distance between the first-order delta functions and the origin, $1/r$, corresponds to the fundamental frequency of the mosaic and is equal to the reciprocal of the row spacing. Only the first and second order delta functions are shown, though the complete spectrum contains higher order delta functions as well.

in each of three orientations. These axes are indicated by arrows around the perimeter of Fig. 1(C). The center-to-center separation between cones, s , corresponds to the spacing between adjacent cones within a row. A more convenient descriptor, which will be adopted here, is the spacing between rows of cones, r , which equals $s\sqrt{3}/2$.

Figure 1(D) shows the amplitude of the Fourier transform of the lattice of cone centers. Like its counterpart in the spatial domain, it is also a triangular lattice. The delta function at

the origin is surrounded by an inner ring of six delta functions, which I will refer to as the *first-order delta functions* of the mosaic spectrum. The distance between the origin and any first-order delta function is equal to $1/r$, which corresponds to the fundamental spatial frequency, or first harmonic, of the photoreceptor mosaic.

The consequences of imaging an interference fringe on this idealized mosaic is first described in the spatial domain: the process of sampling the fringe corresponds to multiplying the distri-

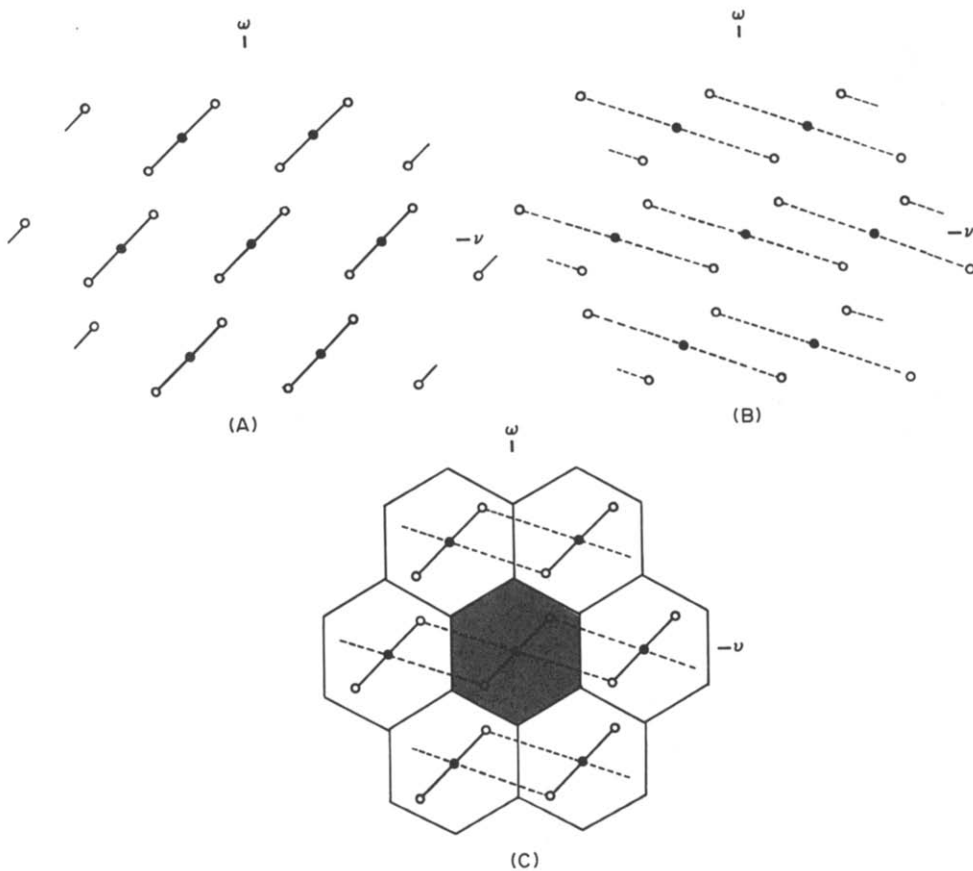


Fig. 2. (A) Representation in the 2-D frequency plane of the triangular lattice sampling the interference fringe depicted in Fig. 1. Black dots represent the delta functions of the original mosaic spectrum. For a lattice of infinitely small sample points, there exists an infinite number of delta functions in the mosaic spectrum, only the central seven of which are depicted. White dots represent the first order delta functions of the original fringe spectrum. The process of sampling the fringe has produced replicas of the fringe spectrum at each of the delta functions of the mosaic spectrum. Solid lines connect the corresponding first-order spectra of each replica. (B) The same spectrum as shown in (A), but produced by convolving the spectrum of the mosaic with the spectrum of another sinusoidal grating of higher spatial frequency and different orientation. Dotted lines connect the corresponding first order delta functions of the original fringe spectrum. The many-to-one mapping of stimuli to mosaic output represents the information lost by sampling, since there is an infinite number of fringes that will produce exactly the same distribution of intensity at each sample point. (C) The spectrum of (A) and (B) has been replotted along with the window of visibility, the shaded hexagon centered at the origin that shows that area of the frequency plane that the postreceptoral visual system can pass. The surrounding six hexagons represent "first-order windows". If the original fringe had been that depicted by the dotted line at the origin, the first-order delta functions of the fringe spectrum fall outside the zero-order window and into the first order windows.

A low frequency alias, shown by the solid line would be passed by the window.

bution of intensity in the fringe by the array of cone locations. This multiplication produces the moiré patterns that are the entoptic fingerprint of the cone mosaic. The equivalent operation in the spatial frequency domain is as follows: the Fourier transform of the interference fringe is convolved with the Fourier transform of the array of cone centers to yield the Fourier transform of the response of the mosaic. The result of this convolution can be seen in Fig. 2(A), which shows the frequency representation of the fringe in Fig. 1 sampled by a triangular lattice. The sampling operation corresponds to erecting a replica of the fringe transform at each of the delta functions in the transform of the mosaic. Solid points indicate the locations of the original delta functions in the mosaic transform. Circles indicate the first-order delta functions of the fringe spectrum, now replicated at each delta function in the mosaic spectrum. Solid lines have been drawn to connect the corresponding first-order spectra of each replica.

Note, however, that exactly the same spectrum would result had the mosaic sampled the fringe whose corresponding first-order delta functions are linked by the dotted lines shown in Fig. 2(B). This fringe has a much higher spatial frequency and a different orientation, but produces an identical spectrum following the sampling operation. These figures illustrate aliasing, the ambiguity introduced by sampling. This pair of fringes of different orientation and spatial frequency are members of an equivalence

class, all members of which produce identical intensity distributions at the lattice points.

The window of visibility

Ultimately, the post-receptoral visual system adopts an interpretation of this ambiguous distribution of quantum catches. The rule for selecting an interpretation is incorporated in the model with a "window of visibility" that specifies the area in the two-dimensional spatial frequency domain to which the post-receptoral visual system is sensitive. The specific window chosen in the model implements the assumption made here that the visual system always adopts the lowest spatial frequency interpretation of the stimulus. Observations of spatial frequencies near the foveal Nyquist limit (Williams, 1985b) suggest that this rule is probably roughly correct.* This rule is to be expected since, under everyday viewing conditions, diffraction and aberrations in the optics of the eye confine visual experience to low spatial frequencies. The window that exactly captures the rule is a hexagonal-shaped area, centered on the origin, whose boundaries lie nearest the origin at a spatial frequency of $1/2r$ (Mersereau, 1979). This window is shown as the shaded area in Fig. 2(C). The edge of the window corresponds to the Nyquist limit of one-dimensional sampling theory.

The window of visibility, or zero-order window, is surrounded by six *first-order windows*, one centered on each of the first-order delta functions of the mosaic spectrum. To understand aliasing in the framework of this model, first consider fringes whose first-order spectra fall within the window. They have high frequency aliases, but they are not passed by the window, which passes only the original low frequency fringe. However, high spatial frequencies whose first-order spectra lie outside the zero-order window will produce delta functions that fall within the window. These delta functions will be reconstructed as a low frequency alias.

Basis for the psychophysical procedure

The model above assumes that the cone mosaic is a crystalline lattice. It is only under these conditions that the moiré patterns produced by the mosaic should be regular. A disordered mosaic does not have a discrete amplitude spectrum: the delta functions in the mosaic spectrum become blurred with small amounts of disorder. This blur in turn leads to distortion in the moiré

*However, the precise boundaries of the window actually employed by the visual system have yet to be carefully mapped, and the window proposed here is probably inaccurate in several ways. For example, the window has an abrupt edge that neglects the gradual neural loss in interference fringe contrast sensitivity with increasing spatial frequency (Williams, 1985b). Furthermore, there is no evidence that the window has a hexagonal shape. Indeed, the existence of the oblique effect suggests that the true shape is better approximated by a diamond than a hexagon. There is no unique window for reconstructing signals that have been sampled in two dimensions (Peterson and Middleton, 1962). The hexagonal window was chosen because it is optimal for reconstructing signals with isotropic two-dimensional power spectra and because an array of such windows completely tiles the frequency plane. For the present purpose of mapping the foveal cone mosaic, the behavior of the window at its edges is of little consequence. This is because the psychophysical observations described later in the paper that support the model are strictly supra-threshold, and involve relatively low spatial frequency moiré patterns that fall near the center of the window rather than at its edges.

patterns that are produced, since the moiré patterns have blurred spectra as well. Support for a crystalline lattice structure of the cone point pattern may be obtained from experimental evidence for the existence of these delta functions, which would imply substantial regularity in the foveal cone mosaic. The model above assumes that the cone mosaic is not only regular but also forms a triangular crystalline lattice. This leads to specific predictions about the behavior of moiré patterns that would be different if, for example, the cones were packed in a rectangular array.

The coordinates of the six first-order delta functions in the spectrum of the triangular lattice contain rich information about the mosaic itself. The distance between these delta functions and the origin specify the spacing between rows of cones in the mosaic. The number of first-order delta functions and the angles between them with respect to the origin specify the packing geometry. If the coordinates in the frequency plane of these delta functions could be identified with a psychophysical procedure, then the spacing and packing geometry of the mosaic could be characterized.

One way to identify these coordinates is to find those interference fringes that produce what will be called a *moiré zero*. A moiré zero occurs when a fringe of some orientation and spatial frequency produces a moiré pattern of zero spatial frequency. The Appendix derives a quantitative description of the dependence of the spatial frequency of the alias on the spatial frequency and orientation of the interference fringe stimulus. Only the essential intuition is described here.

Consider an interference fringe whose

first-order spectra fall somewhere beyond the zero-order window and within the ring of first-order windows in Fig. 2. This fringe will produce an alias that will pass through the zero-order window. It can be seen from the geometry that a moiré zero will occur anytime the first-order delta functions in the fringe spectrum fall on the first-order delta functions of the mosaic spectrum. Interference fringes whose spectra do not cause this to happen will always produce an alias of spatial frequency higher than zero. For the triangular lattice implemented in the model, a moiré zero can occur only for a fringe of a fixed spatial frequency, corresponding to the reciprocal of the spacing between rows of cones in the lattice, $1/r$.^{*} In addition, a moiré zero can occur only if the fringe is oriented at one of three orientations relative to the lattice. That is, the fringe must be oriented parallel to one of the three cardinal axes of the triangular lattice.

The behavior of the moiré zeroes described above for a triangular lattice is restated below in the form of two predictions. The reason for casting the predictions in this form is that the two predictions are tested separately with psychophysical experiments described in Sections II and III below.

(1) *The apparent spatial frequency of the moiré pattern will be lowest when the period of the fringe equals the spacing between rows of cones.* Strictly speaking, the model predicts that a moiré zero will occur when the period of the fringe equals the spacing between rows of cones only if the fringe is oriented parallel to rows of cones that form a triangular lattice. However, the argument is made in the Appendix that this prediction should be approximately correct regardless of the orientation of the interference fringe relative to the mosaic.

(2) *If the period of a fringe equals the spacing between rows of cones in a triangular lattice, then a moiré zero will occur at three orientations of the fringe separated by 60 deg. These orientations will correspond to the cardinal axes of the lattice.* Following a description of the methodology common to all the experiments, Section II provides a test of the first prediction of the model by securing psychophysical estimates of cone spacing across the central fovea for comparison with anatomical measurements. The second prediction is tested in Section III, and allows psychophysical measurement of the packing geometry and orientation of the mosaic at the foveal center.

^{*}This analysis ignores the possibility of moiré zeroes produced by fringes whose spectra fall on higher-order delta functions of the mosaic spectrum. We have thus far been unable to muster any compelling psychophysical evidence for the existence of such higher-order aliases, probably because the required spatial frequency of the stimulus is so high that it is severely demodulated. Low pass filtering by the cone aperture, and perhaps the high temporal frequency of the alias produced by eye tremor, probably obliterate this effect. As will be seen below, the first moiré zero occurs at 112 c/deg, averaged across observers, at the foveal center. The lowest spatial frequency that could produce a moiré zero from the second-order ring of windows would be 194 c/deg, which is well beyond the highest frequencies at which aliasing has been reliably observed (150–160 c/deg, Williams, 1985a).

General Method

All experiments described in this paper were performed with a computer-controlled laser interferometer described by Williams (1985a). The source was a 632.8 nm, helium-neon laser. Fringe spatial frequency was controlled by varying the separation of a pair of coherent point sources imaged near the entrance pupil of the eye. The point sources were always symmetrically placed relative to the Stiles-Crawford maximum in the entrance pupil. Fringe orientation was controlled by a reversion prism placed just behind the field stop that was conjugate with the observer's retina.

Interference fringes were introduced and removed from a uniform coherent field without changing the space-averaged retinal illuminance. This was achieved with the pulse overlap technique described by Williams (1985a). Briefly, the two beams of the interferometer were gated independently to produce pairs of light pulses 1 msec in duration 400 times a second. The temporal overlap of the pulse pairs could be manipulated by computer to modify the contrast of the fringe: no temporal overlap produced a fringe of zero contrast while complete overlap produced a unity contrast fringe of the same space-averaged illuminance. In all experiments, unity contrast interference fringes were presented for 500 msec every 2.5 sec. The two second interstimulus interval reduced habituation effects that can occur with steady viewing, and also helped the observer distinguish between aliasing and the speckle that characterizes coherent fields imaged on the retina. Unless otherwise stated, the retinal illuminance of the display was 2000 td.

Dental impressions were used to maintain head position relative to the apparatus. The alignment procedure used is described by Williams (1985a). Prior to each experimental session, tropicamide (1/2%) was used to dilate each observer's pupil (except in the case of one observer, N.C.). This helped to ensure that the point sources that formed the interference fringe were never occluded by the iris. Observers ranged in age from 20 to 37 years of age and had normal vision except for the correction of mild myopia and astigmatism. Observer K.K. is a protanope though his vision appears to be normal in other respects.

II. CONE SPACING ACROSS THE HUMAN FOVEA

The first experiment employs the zebra stripe

patterns to measure cone spacing across the human fovea. The first prediction listed above suggested that, at any one retinal location, the observed moiré pattern should have the lowest spatial frequency when the interference fringe period equals the spacing between rows of cones. The Appendix establishes the predicted dependence of the moiré spatial frequency on the spatial frequency of the interference fringe (Fig. 11). If observers are asked to adjust the spatial frequency of an interference fringe to make the moiré pattern as coarse as possible at any retinal location, the reciprocal of their setting should agree with anatomical estimates of cone spacing. Williams (1985a) used this technique to measure cone spacing at the foveal center, and found that the psychophysical observations and anatomical measurements were in reasonable agreement. The present paper adapts this technique to measure cone spacing across the fovea as well as at the very center.

Williams (1985a) reported that interference fringes that can just be resolved at the very center of the fovea produce an annular moiré pattern surrounding the center of fixation. The appearance of this annulus is depicted in Fig. 3. The diameter of the annulus shrinks with increasing spatial frequency, finally collapsing to a disk of zebra stripes at a frequency of about 90 c/deg. The drawing fails to capture the low apparent contrast of the zebra stripes and the

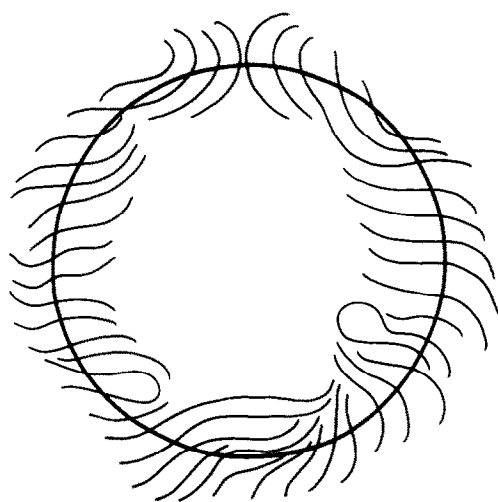


Fig. 3. Appearance of the annulus of zebra stripes when it is matched in size to a faint bright ring (radius = 0.75 deg) superimposed on the test field. The drawing fails to capture the scintillating appearance of the zebra stripes, as well as their relatively low apparent contrast. The spatial frequency of the fringe was 75 c/deg and the orientation was horizontal (observer: N.C.).

fact that they scintillate rapidly in time, perhaps as a result of eye movements. One explanation for the annulus is that it marks the retinal locus at which the spacing between rows of cones matches the period of the interference fringe. The increase in the diameter of the annulus with decreasing spatial frequency would then reflect the increase in cone spacing with increasing eccentricity from the foveal center.

Annulus matching technique

The following technique was designed to obtain a quantitative test of this explanation. Observers viewed a dim ring of 630 nm light centered on a test field in which the interference fringe was periodically presented. The test field was at least 4 deg in diameter. The ring was introduced via a beamsplitter and was produced by passing incoherent light from a tungsten source through a photographic transparency. The thickness of the ring was 2.5 min of arc. At the beginning of each run, the observer adjusted the intensity of this ring so that it was just bright enough to be clearly seen but dim enough not to interfere with the visibility of the zebra stripes. The observer's task was to fixate the center of the ring and adjust the spatial frequency of the interference fringe till the coarsest zebra stripes fell on the ring, as shown in Fig. 3. This was done for rings of different radii, providing a way of varying eccentricity from the foveal center. To make measurements at the foveal center, the ring was removed, and the observer was instructed to adjust the spatial frequency until the zebra stripes were coarsest at the point of fixation. The order in which rings of different radii were tested varied randomly within each session. Two settings were made for each ring before proceeding to the next ring.

Results

Measurements were attempted on nine observers in all. Table 1 shows the results for eight of these observers as well as details regarding the experimental conditions used. Reliable data could not be obtained on one observer. She reported a scintillating annulus outside the region over which she could resolve the fringes but could not identify wavy stripes within the annulus with certainty. A second observer (I.W.) had difficulty seeing zebra stripes with vertical interference fringes, though reliable data were obtained for horizontal fringes. Five observers readily identified the annulus of zebra stripes, and made settings with some confidence. For two additional observers (J.H. and R.S.), measurements were made only at the foveal center. No observer could make reliable measurements with this technique for retinal eccentricities larger than about 1.75 deg. For ring radii beyond about 1.25 deg, the zebra stripes begin to degenerate into a much less clearly defined annulus of two-dimensional noise.

The solid symbols in Fig. 4 show the mean fringe period yielding the coarsest zebra stripes for all eight observers as a function of foveal eccentricity. The error bars represent ± 1 SD based on variability between observers. Measurements were made at two different fringe orientations for five of the observers; the geometric mean of the settings for the two orientations was calculated to provide a single estimate of cone spacing at each eccentricity for each observer.

These data are compared with the anatomical data of Österberg (1935), shown as the solid line, and the mean data ($n = 4$) of Curcio *et al.* (1987), shown as the dotted line. Both sets of

Table 1. Estimates of cone spacing in minutes of arc as a function of retinal eccentricity for the foveas of 8 observers

Observers	Retinal eccentricity (deg)										Fringe orientation (deg)	Retinal illumination (td)	N
	0.00	0.25	0.375	0.5	0.625	0.75	1.0	1.25	1.5	1.75			
D.W.	0.53	0.56	0.65	0.74	0.79	0.84	0.97	1.08	1.16	1.33	0, 90	2000	8
M.D.	0.51	0.58	0.64	0.70	0.76	0.82	0.95	1.07	1.14	1.21	0, 90	2000	8
N.C.	0.52	0.58	0.63	0.67	0.75	0.82	0.89	1.01	1.07	1.16	0, 90	500	8
P.L.	0.51	0.59	0.65	0.74	0.81	0.84	0.93	1.01	—	—	0, 90	2000	4
K.K.	0.54	0.56	0.61	0.69	0.75	0.83	1.00	1.03	—	—	130, 160	4000	4
I.W.	0.53	0.55	0.59	0.70	0.77	0.84	—	—	—	—	90	2000	4
R.S.	0.57	—	—	—	—	—	—	—	—	—	90	2000	4
J.H.	0.57	—	—	—	—	—	—	—	—	—	90	2000	2
Mean	0.535	0.570	0.628	0.707	0.772	0.832	0.948	1.04	1.123	1.233			

Each table entry represents the mean measurement of cone spacing in minutes of arc for a single observer at a single retinal eccentricity. For observers in which two orientations were tested, the data for both orientations are averaged. N equals the total number of observations for each table entry. The convention for fringe orientation is 0 deg = vertical, increasing counterclockwise. The right eyes were tested of all observers except I.W.

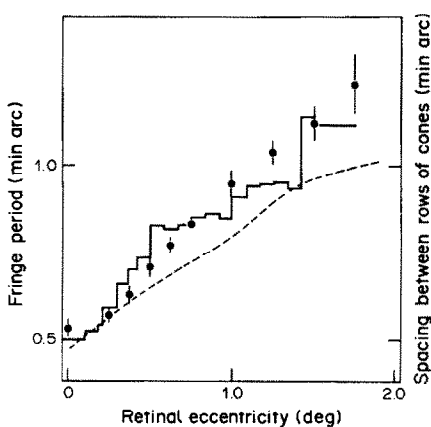


Fig. 4. Solid symbols show the period of the interference fringe that produced the coarsest zebra stripes at various retinal eccentricities within the fovea. Results are the mean of from 3 to 8 observers, depending on retinal eccentricity, whose individual results are tabulated in Table 1. Error bars represent ± 1 SD based on variability between observers. The solid line represents data from Österberg (1935) in the temporal retinal meridian and the dotted line represents the mean data for 4 eyes for both nasal and temporal meridians taken from Curcio *et al.* (1987).

anatomical data were originally expressed in cones/mm² whereas the psychophysical data are expressed in minutes of arc. To compare the data, the angular spacing between rows of cones, r , in min of arc was calculated from the anatomical measures of cone density, D , in cones/mm² by assuming triangular packing:*

$$r = (60/0.291)(\sqrt{3/2D})^{1/2}.$$

There is reasonable agreement between the psychophysical observations and the measurements of Österberg. The mean data of Curcio *et al.* rise somewhat more slowly than the psychophysical data but the meaningfulness of this difference is difficult to evaluate due to the large individual differences reported by Curcio *et al.*

For clarity, the psychophysical data are compared with only two sets of human anatomical

*The factor of 0.291 converts mm of retinal distance to degrees of visual angle, and is taken from LeGrand's theoretical eye (Wyszecki and Stiles, 1982). The conversion factor varies from eye to eye and is not available for the specific eyes studied. Other representative values have been suggested such as about 0.275 mm/deg (Drasdo and Fowler, 1974). Adopting this value would raise all the anatomical data by about 6% relative to the psychophysical data, and improve the overall fit. Österberg's tabulated data on cone spacing contain numerous errors that have been perpetuated in the literature. These errors can be resolved by comparing Österberg's tables with his corresponding graphs (Rodieck, 1986).

data in Fig. 4. However, recent measurements of cone spacing in the monkey (de Monasterio *et al.*, 1985; Hirsch and Miller, 1987; and Perry and Cowey, 1985) are also in good agreement with the psychophysical data though the angular cone spacing is somewhat larger in the monkey largely as a result of the smaller axial length of monkey eyes. The psychophysical estimate of row spacing at the foveal center, 0.535 min of arc, is also in close agreement with the human anatomical estimate of Miller (1979), which was 0.536 min of arc. Overall, the agreement supports the hypothesis that aliasing can provide a measure of cone spacing in the living human eye.

There is evidence for an anisotropy in cone spacing in those observers for which spacing was measured for more than one orientation. Figure 5 shows individual data for four observers for which measurements were obtained for both horizontal (open symbols) and vertical gratings (solid symbols). Curiously, the fringe period yielding the coarsest zebra stripes is consistently larger when the fringe is vertical than when it is horizontal. This effect is present in all the observers though observer P.L. shows it less strongly than the others. The fringe period yielding the coarsest zebra stripes averaged across retinal locations is 17.4, 2.5, 19.5, and 14.8% larger for vertical than horizontal fringes for observers D.W., P.L., M.D., and N.C. respectively.

Additional measurements of this phenomenon were obtained on observer D.W. with a

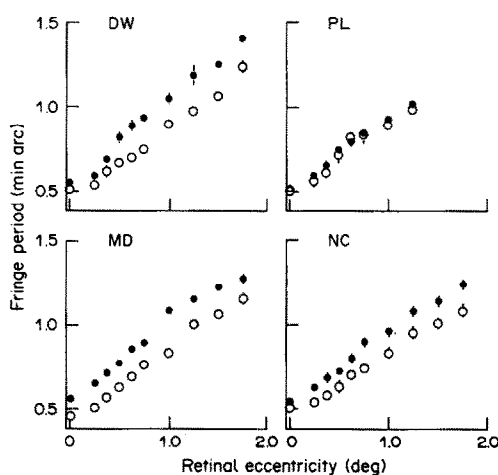


Fig. 5. Comparison of annulus matching data for horizontal (open symbols) and vertical (solid symbols) interference fringes for four observers, showing evidence for a local anisotropy in cone spacing. Error bars represent ± 1 SEM based on variability between runs.

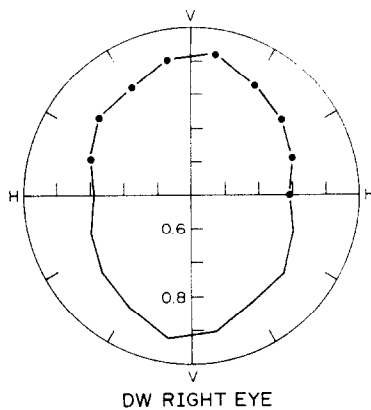


Fig. 6. Period of interference fringe producing the coarsest zebra stripes at an eccentricity of 0.75 deg, as a function of fringe orientation. The origin corresponds to a fringe period (and predicted cone spacing) of 0.5 min of arc, the perimeter corresponds to 1.0 min of arc. Since vertical fringes estimate the horizontal separation between cones and vice versa, the data imply that the horizontal cone separation is 1.16 times larger than the vertical cone separation in this observer. Error bars representing plus and minus one standard error of the mean are smaller than the data points.

matching ring of radius, 0.75 deg. Two settings were made at each of 9 fringe orientations in 20 deg steps from 0 to 180 deg. The symbols on the polar plot of Fig. 6 show the mean fringe period that produced the coarsest zebra stripes on the matching ring. The center of the plot corresponds to a fringe period of 0.5 min of arc, the perimeter corresponds to a fringe period of 1 min of arc. The full range of possible stimulus orientations are covered in only 180, so that the 360 deg polar plot exhibits obligatory 180 deg rotational symmetry. The data form a relatively smooth ellipse, with the major axis corresponding to vertical gratings. The aspect ratio of the ellipse is about 1.16. The implications of this anisotropy are treated in the Discussion, where it is argued that foveal cones in these observers must be more tightly packed in a vertical than a horizontal direction.

III. PACKING ARRANGEMENT OF FOVEAL CONES

The following experiments seek psychophysical evidence for the packing geometry of cones by attempting to identify the cardinal axes of the mosaic at the point of fixation. The second prediction of the model of cone aliasing is that if the fringe spatial frequency is fixed at the mosaic fundamental frequency, a moiré zero should be encountered with every 60 deg of fringe rotation. The predicted change in moiré spatial frequency with fringe orientation is

established in the Appendix (Fig. 12). An interference fringe of about 112 c/deg corresponds to the fundamental frequency of the mosaic at the foveal center, as determined in the previous experiment. If this fringe is rotated, the moiré spatial frequency should oscillate between 0, corresponding to a moiré zero, and 58 c/deg with a period of 60 deg.

This prediction is simulated in Fig. 7 with a technique introduced by Yellott (1982). The foveal section used for the simulation was prepared by William Miller and Joy Hirsch at Yale University. Dots in each panel represent the locations of cone centers within the central 0.5 deg of the monkey fovea. Each mosaic is sampling a square wave grating whose period equals the spacing between rows of cones at the foveal center. The effects of six different orientations are shown, spanning the range of possible orientations in 30 deg steps. The upper row of sampled gratings represent the three moiré zeroes corresponding to the cardinal axes of the lattice. The moiré patterns in the lower row of sampled gratings are much higher in average spatial frequency, corresponding to conditions in which the stripes of the grating are oriented between cardinal axes.

Method

Two psychophysical procedures were used to search for the fringe orientations that yielded moiré zeros.

Rating Technique. Observers viewed a 2 deg coherent test field surrounded by an 8 deg equiluminous annulus of incoherent 630 nm light. A crosshair, visible only in the annulus, was centered on the test field. Its purpose was to aid fixation and to reduce torsional eye movements. The fringe spatial frequency was set at that frequency yielding the coarsest zebra stripes at the center of fixation. This frequency varied slightly from observer to observer, but fell within the range of 105–119 c/deg. The observer's task on each trial was to rate the overall coarseness of the zebra stripes on a scale of 1 to 10, with 10 representing the coarsest and 1 the finest. Observers were instructed to make their rating on the basis of the smallest area lying at the center of fixation to which they could direct their attention. Observers were allowed an unlimited number of fringe presentations upon which to base their rating. A fringe of a different orientation was presented on each trial. Fringes at eighteen orientations, spanning the range of possible orientations in 10 deg steps, were

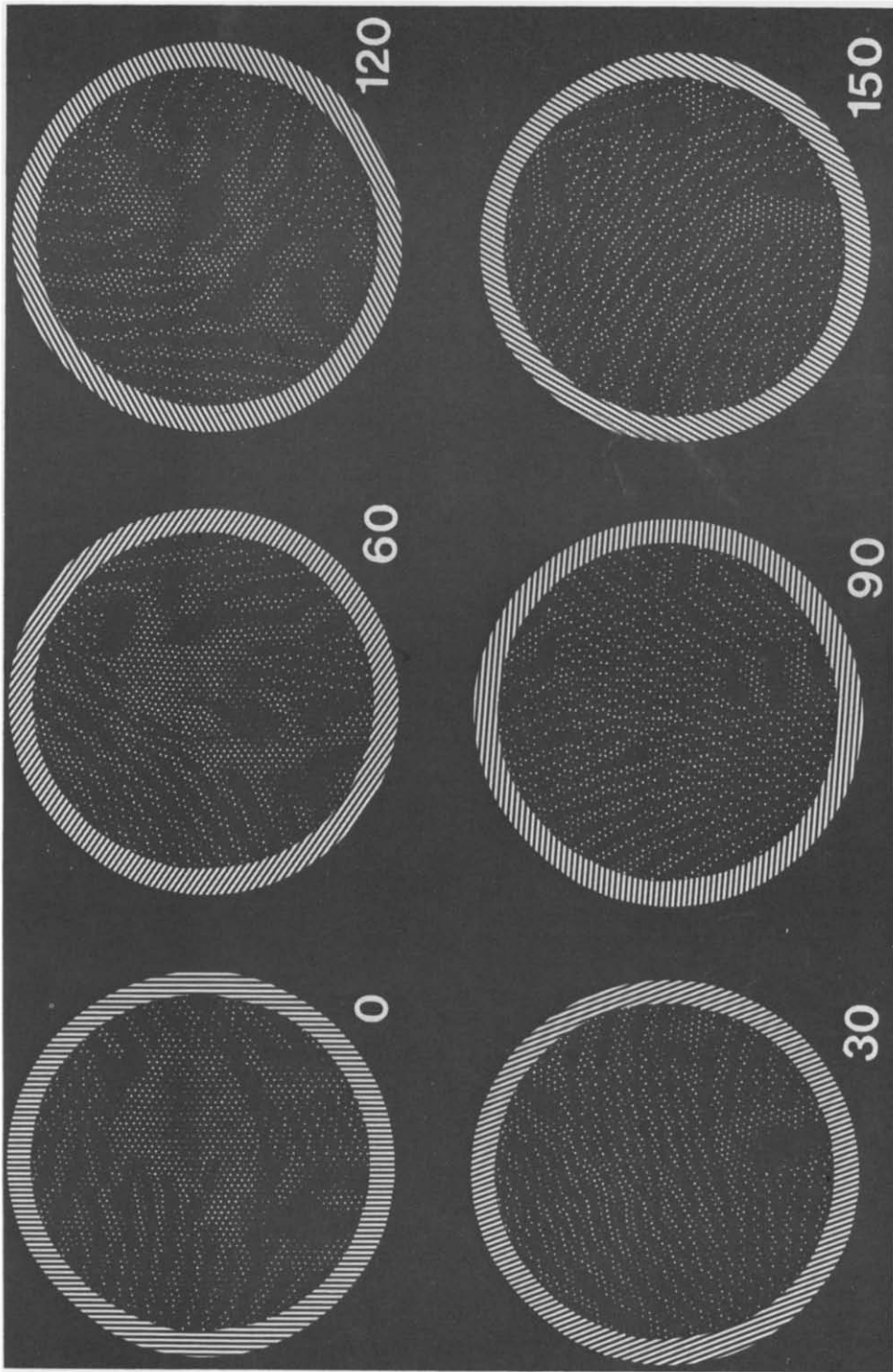


Fig. 7. Simulation of the effect of fringe orientation on the coarseness of the resulting moiré pattern, demonstrating that the foveal mosaic is sufficiently regular to produce effects roughly consistent those expected from a crystalline lattice. Each panel shows the central $1/2$ deg of the primate fovea sampling a square wave grating whose period matches the row spacing of the mosaic. Gratings whose orientations are 0, 60, and 120 lie parallel to one of the cardinal axes of the mosaic; gratings whose orientations are 30, 90, and 150 lie between cardinal axes. Moiré zeroes are simulated in the upper three panels, which show a coarser moiré pattern than that seen when the gratings are misaligned with the mosaic, as shown in the lower three panels.

presented in random order within each run.* At least four ratings were obtained at each orientation for each eye tested. Both the left and right eyes of three observers were tested, as well as the right eyes of two additional observers.

Orientation adjustment technique. The stimulus display was similar to that used in the rating technique. As before, the spatial frequency was fixed at the fundamental frequency of the mosaic at the foveal center. Observers searched for a moiré zero by adjusting the orientation of the interference fringe so that the spacing of zebra stripes was largest at the very center of the fovea. Fifty settings were made in a session. The left and right eyes of two observers were tested.

Results

Figure 8 shows the results of the rating technique for all eyes tested. Fringe orientation is indicated around the circumference of each plot. The mean rating at any orientation is given by the distance of the data point from the origin. The circle at the center corresponds to the smallest permissible rating, 1, and the outer circle has a radius of 10, the highest permissible rating. Error bars represent ± 1 SEM. The data points have been plotted only around the upper half of the 360 deg plot because 180 deg of stimulus rotation includes all possible fringe orientations. This gives the complete polar plot 180 deg rotational symmetry. Moiré zeroes should correspond to orientations where the ratings are highest, orientations between moiré zeroes should produce low ratings. Triangular packing would predict moiré zeroes every 60 deg, or a 6 pointed "starfish" pattern in the plot.

Figure 9 shows the results of the orientation adjustment technique. The 50 orientation settings made by each observer with each eye were tallied in 5 deg bins to yield a polar histogram. The ring at the center of the plot corresponds to zero settings per bin; the radius of the plot is 13 settings per bin. The results of the rating technique for these same eyes are plotted as dotted lines for comparison.

*Observers could potentially deduce the true orientation of a fine interference fringe from an artifact produced by a refractive error. Refractive errors cause the retinal test fields arising from each point source in the pupil to fall slightly out of register. They are typically displaced slightly along a line perpendicular to the orientation of the fringe. Refractive errors and astigmatism were corrected with trial lenses to minimize this problem. At the end of the experiment, all observers except the author claimed that they had been unaware of the true orientation of the high frequency fringe on each trial.

The data for some of the eyes, such as those of P.L. and D.W., reveal the clear signature of triangular packing. For these observers, a moiré zero could be identified by a relatively coarse pattern of zebra stripes meandering across the foveal center. Orientations between moiré zeroes were characterized either by very fine zebra stripes of low apparent contrast, or by a relative paucity of zebra stripes at the foveal center. Under these conditions the foveal center had a flickering, desaturated appearance resembling the appearance of interference fringes at the fovea that are just above the resolution limit. It was usually the case that more coarse zebra stripes were visible in adjacent areas of the fovea, making it important for observers to make their judgements only with regard to the very center of the fovea.

For other eyes, the six-armed starfish pattern is not as obvious from simple inspection, and a more elaborate analysis was employed to evaluate any 60 deg periodicity. The amplitude and phase of the discrete Fourier series of each data set was computed. Due to the periodic nature of the data, and its obligatory 180 deg rotational symmetry, the only Fourier components that could appear in the data (in addition to a d.c. term) had periods of $180/n$ deg, where n is an integer greater than or equal to 1. In 6 of the 8 eyes tested with the rating technique, the harmonic with the largest amplitude had a period of 60 deg. Even in the remaining two eyes (M.D., left eye and J.H., right eye), the 60 deg harmonic had the second largest amplitude, with the 180 deg harmonic having the largest amplitude. The 60 deg harmonic was largest for all four of the eyes tested with the orientation adjustment technique. The phase of the 60 deg harmonic is indicated by the six arrows surrounding each plot in Figs 8 and 9. Note in Fig. 9 that the two different techniques applied to the same eyes generally yield similar estimates of the orientation of the triangular mosaic.

The 60 deg periodicity in these data originates in the observer's visual system, and is not some peculiar artifact of the laser interferometer. The author verified this by repeating the rating technique while lying down on a tabletop with his bite bar rotated 90 deg in its mount. The dotted line plotted in Fig. 8 for the right eye of D.W. shows the result: the arms of this starfish are interdigitated with those obtained with the observer upright, suggesting that the starfish has apparently rotated with the eye. This is consistent with the hypothesis that the effect arises in

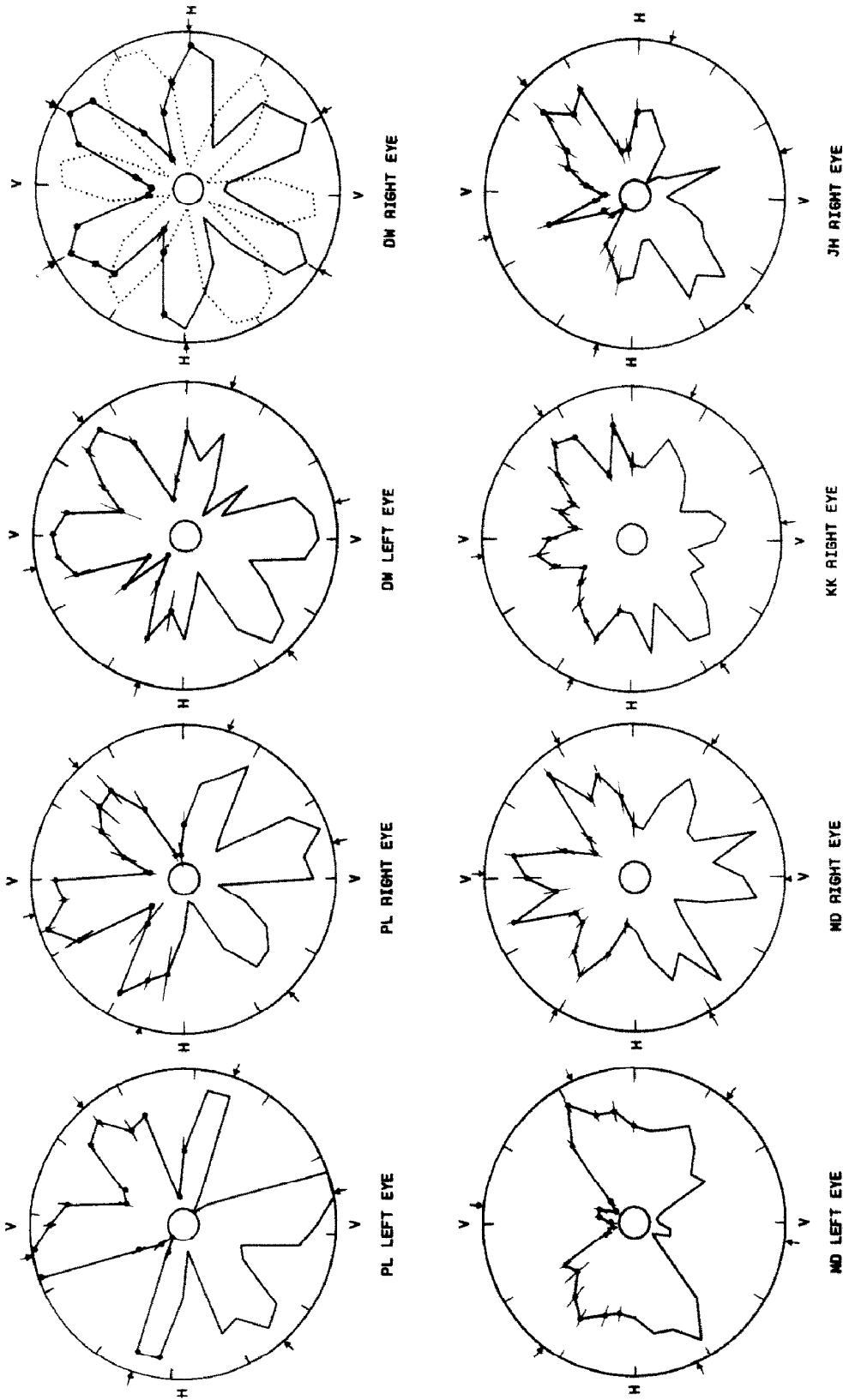


Fig. 8. Results of the rating technique for 8 eyes (5 observers). Each panel shows the mean rating of the coarseness of zebra stripes as a function of fringe orientation, when the fringe spatial frequency was set close to the fundamental frequency of the mosaic at the foveal center. Error bars represent ± 1 SEM based on variability between runs. Arrows at the perimeter of each plot show the orientation of the component with a 60 deg period, extracted from the data by a discrete Fourier series. These arrows provide an estimate of the orientation of the lattice at the foveal center. The dotted line in the upper right panel represents a control experiment showing that the 60 deg periodicity in the data arises in the visual system of the observer and not in the apparatus.

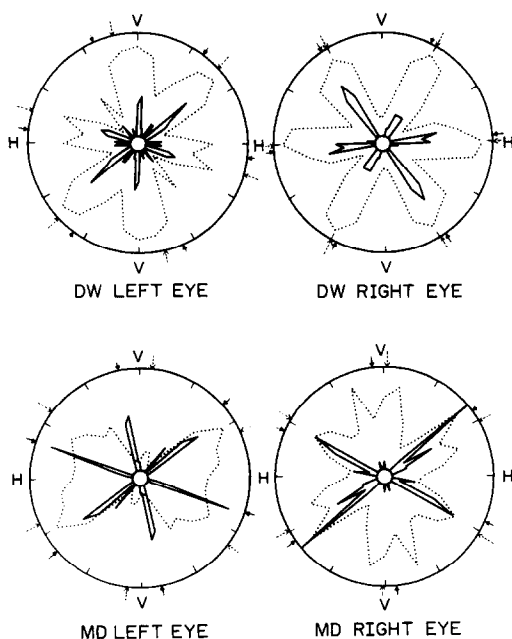


Fig. 9. Results of the orientation adjustment technique to establish the orientation of the cone mosaic at the foveal center. Left and right eyes of two observers are shown. Results of the rating technique from Fig. 8 on the same eyes are shown for comparison.

the visual system and not the apparatus. Furthermore, the observer could identify the idiosyncratic pattern of zebra stripes for particular orientations, and these patterns were stable in retinal coordinates and not in apparatus coordinates as the head was rotated 90 deg.

DISCUSSION

The estimates of cone spacing obtained with the moiré technique agree reasonably well with those obtained with conventional anatomical methods, which tends to validate both. The psychophysical data show less variability between observers than the anatomical data of Curcio *et al.* (1987). The spacing between rows of cones at the foveal center for the 4 eyes studied by Curcio *et al.* ranged from about 0.39 to 0.69 min of arc, whereas the range for the 8 psychophysical observers was between 0.51 and 0.57 min of arc. A better comparison of these two sets of data could be made if the axial length of the eyes were known to allow distance on the retina to be converted more accurately to visual angle. If foveal cone spacing in mm

covaried with the eye's axial length, some of the variability observed in the anatomical data would disappear when expressed in angular terms. On the other hand, the variability observed by Curcio *et al.* (1987) is largely confined to the fovea, whereas variations in axial length would have about the same impact at all eccentricities, arguing against this explanation. The population sampled in the two studies are likely to be different. Clearly more ambitious psychophysical and anatomical studies on a larger number of eyes will have to be done to determine the variability in cone spacing in the population at large.

The agreement between psychophysical and anatomical estimates of cone spacing across the central fovea argues against competing pre-receptor or post-receptor explanations for the zebra stripes. An explanation in terms of cone aliasing is further strengthened by the identification of 60 deg symmetry in the pattern producing the zebra stripes. This makes it unlikely that the zebra stripes arise as a result of some optical effect of the neural tissue overlying the receptors, which lacks the necessary crystalline structure. Aliasing at a higher stage in the visual system, such as at the array of ganglion cell receptive fields, is not required to explain the observations. This is consistent with anatomical evidence that there are sufficient numbers of ganglion cells to adequately sample the primate cone mosaic (Perry and Cowey, 1985).

The appearance of the zebra stripe patterns are apparently quite stable over time. The author has been unable to detect a change in the appearance of a horizontal fringe of 110 c/deg over a period of three years, as would be expected if the zebra stripe is a consequence of retinal anatomy. Observers quickly learned to recognize the zebra stripe patterns associated with a particular stimulus and often remarked that they recalled a particular pattern experienced during a previous experimental session. For a given fringe, the zebra stripes are probably as idiosyncratic as a fingerprint. The appearance of the pattern is also stable with changes in the entry point of light in the pupil, except at large pupillary eccentricities where the apparent contrast is reduced. Changes in the wavelength of the fringe do not noticeably alter the form of the zebra stripes, provided the fringe spatial frequency and orientation is kept constant. The author has observed zebra stripes across most of the visible spectrum by using different laser sources; a helium-cadmium laser (442 nm), an

argon laser (488 and 514 nm), a dye laser (540–575 nm), and helium–neon (632.8 nm).*

The 632.8 nm light used throughout the measurements reported here is absorbed only by the middle and long wavelength cones, and negligibly by the short wavelength cones. Thus, the estimates of cone spacing are based on only two of the three cone types in the human fovea. However, the short wavelength cones account for at most only 10% of the total cone population in the primate (Marc and Sperling, 1977; de Monasterio *et al.*, 1985). Simulations show that the psychophysical measure of cone spacing should be relatively immune to the absence of short wavelength cones. Lattices constructed from photographs of the primate foveal cone mosaic that have cones deleted suggest that removal of 10% of the cones does not obviously disrupt the visibility of the moiré zeroes. More importantly, it does not change the spatial frequency at which moiré zeroes occur at all. Ahumada (1986) has demonstrated this last point with regard to the aliasing effects expected from the separate mosaics of middle and long wavelength cones.

A minority of observers, such as the one who was dropped from the experiment to measure cone spacing, have been unable to observe the zebra stripes. These observers report the appearance of a rapidly flickering, desaturated patch centered on fixation just like the observers who resolve the zebra stripes. The size of this patch decreases with increasing spatial frequency. It is not clear what factors allow some observers to see the stripes and others not, though it may be related to individual differences in the amplitude of eye tremor which would tend to reduce the contrast of the zebra stripes in some eyes more than others. Whatever the cause, it restricts the population of observers for which foveal topography can be mapped with this technique.

Ideally, it would be desirable to identify moiré zeroes with two-alternative forced choice measurements of fringe contrast sensitivity, under the assumption that observers would be more sensitive to moiré zeroes than higher frequency aliases. However, forced choice detection procedures, which have the advantage that they are criterion free, are inappropriate in this case. Attempts to use this technique were not successful because observers could detect the presence

of flicker and desaturation in the field regardless of the appearance of the zebra stripes themselves.

Local anisotropy in cone spacing

In the four observers for which cone spacing measurements were made for both horizontal and vertical gratings, moiré zeroes at a particular eccentricity required a spatial frequency that was about 14% higher on average for horizontal fringes than for vertical. The effect is most striking when observing a fine interference fringe of fixed spatial frequency whose orientation is changing smoothly and continuously. The annulus of zebra stripes always remains roughly circular, but it oscillates in size, appearing largest when the fringe is horizontal and smallest when the fringe is vertical.

On the face of it, the most likely explanation for this effect would be an optical one, in which the fringe magnification depended on its orientation. However, the obvious optical causes for such an anisotropy can be excluded. The apparatus had no measurable anisotropic magnification. Measurements of the spacing between the point sources at the pupil, made with a micrometer, confirmed that spatial frequency was independent of orientation within measurement error (less than 0.5%). Furthermore, the effect rotated with the observer when the fringe orientation was fixed and the observer's head was rotated 90 deg, confirming that it arises in the eye.

Astigmatism in the eye's anterior optics, which can make retinal magnification (and spatial frequency) dependent on fringe orientation (meridional aniseikonia), was not large enough to account for the effect. All the observers were mildly myopic and those with astigmatism were most myopic in approximately the horizontal meridian. Astigmatism was 1.5 D for D.W. and P.L., 0.25 for M.D. and virtually 0 for N.C. The amount of meridional aniseikonia expected from these amounts of astigmatism was calculated by ray tracing through Le Grand's full theoretical eye (Wyszecki and Stiles, 1982). These calculations showed that even the most severe astigmatism observed, applied to either the cornea or the lens would produce a magnification difference for vertical and horizontal fringes of less than 0.5%. This is far less than the meridional aniseikonia required to explain the 14% effect, averaged across all retinal locations for all four observers. The minimum amount of astigmatism at a single refractive surface in the eye required to explain

*Though the pattern of the zebra stripes is not altered, their apparent contrast is reduced with shorter wavelength fringes for reasons that are presently unclear.

the effect would be 41 D, applied at the anterior surface of the cornea.*

Furthermore, trial lens correction of the astigmatism for observer D.W. did not significantly change the magnitude of the effect.† The refractive effect of the foveal pit (Williams, 1980) is too small to account for the effect. Because of the relatively small difference in the index of refraction of the vitreous and retina and its proximity to the photoreceptor mosaic, the foveal pit might magnify the foveal image by one or perhaps 2% at most. Any astigmatism it might exhibit would be even smaller still.

It is equally difficult to attribute the anisotropy to postreceptoral factors, such as under-sampling at a subsequent, anisotropic neural stage. All the evidence points to an origin for the zebra stripes in the cone mosaic (Williams, 1985a), and indeed it is difficult to see how the cone mosaic could avoid aliasing under these conditions. At the appropriate spatial frequency, the cone mosaic inevitably generates a low frequency moiré pattern that is easily passed

by subsequent neural filtering. Any hypothetical subsequent stages with anisotropic sampling would be confronted by a pattern that has already been aliased to low frequencies, in which case the anisotropy of its sampling array would probably be irrelevant.

These arguments against optical and post-receptoral explanations for the local anisotropy suggest that it probably reflects a difference in the spacing between cones measured in vertical and horizontal directions. Since vertical gratings provide a measure of the horizontal spacing between cones and vice versa, these results mean that there is a tendency for the spacing between cones to be slightly greater in a horizontal direction than a vertical direction at any retinal location within the fovea.

The possibility of histological artifact makes it difficult to argue convincingly for or against the existence of this proposed packing anisotropy on anatomical grounds [though see de-Monasterio *et al.* (1985) Fig. 1(e)]. It is unclear whether the local anisotropy can be attributed to stresses on the adult fovea or to migrational forces responsible for the development of the fovea (Hendrickson and Yuodelis, 1984), which could be stronger in the vertical direction than horizontally.

This anisotropy is not a natural consequence of a triangular packing arrangement of receptors. The dependence of the fringe spatial frequency producing the lowest frequency moiré pattern on fringe orientation should have a periodicity of 60 deg, as shown in the Appendix. The data of Fig. 6, on the other hand, show only 180 deg periodicity. The anisotropy can be seen at many locations in the fovea despite the likelihood that the local lattice orientations are different in these different locations due to disorder.

The local anisotropy is distinct from a meridional anisotropy in the density of cones with eccentricity from the foveal center, which was rarely observed, at least at smaller eccentricities than 1.75 deg. All observers but one described the annular pattern of zebra stripes as ragged but essentially circular. The shape of the annulus is a direct visualization of an "isospacing" contour, and its predominantly circular shape is consistent with an isotropic distribution of cone spacing about the foveal center. This finding justified the use of a psychophysical procedure that was insensitive to meridional differences. The measurements thus obtained can be considered to represent an average of the cone spacing

*Lesser amounts of astigmatism would be required if there were an axial misalignment of the observer, such that the pair of point sources were not imaged at the nodal point of the eye. The effect of axial misalignment can be approximately calculated as follows. The magnification of an interference fringe is proportional to $1 - d/D$, where d is the distance between the image of the point sources and the nodal point and D is the distance at which the eye is focused (Saleh, 1982). However, this effect is small as long as $d \ll D$. For example, even if the misalignment were as much as -1 cm, which is unlikely, 14 diopters of astigmatism would be required to account for the effect. The relatively minor effect of misalignment was checked with the author's eye, which is about 1.5 D myopic. The spatial frequency producing a moiré zero at an eccentricity of 0.75 deg varied only about 5% over a range of ± 3 cm misalignment of the pupil plane from the images of the point sources.

†However, the absence of measurable astigmatism, such as in observer NC, does not necessarily demand the absence of meridional aniseikonia. It is possible that two or more of the four refracting surfaces in the eye's anterior optics have astigmatism along perpendicular meridians such that they compensate for one another in power, removing astigmatism from the complete eye but still producing meridional aniseikonia. This possibility was explored in the theoretical eye by introducing astigmatism along one axis of the anterior surface of the cornea and along the perpendicular axis of the posterior surface of the lens so as to remove any anisotropy in refractive power but still preserve the overall refractive power of the original theoretical eye. This manipulation also required unrealistic amounts of astigmatism: 22 D of corneal astigmatism in addition to 11 diopters of lenticular astigmatism were needed to produce a meridional aniseikonia of 14%.

along all meridia. Observer N.C. reported that the annulus was slightly elliptical, with the long axis of the ellipse lying in a horizontal direction. On the whole, these observations are consistent with anatomical data (Curcio *et al.*, 1987) for which some eyes showed elliptical isodensity contours oriented as in the eye of N.C. and while others showed circular contours.

Orientation of the cone lattice at the foveal center

On the whole, the orientation rating and adjustment techniques applied to the foveal center provided strong evidence for the 60 deg symmetry predicted by the triangular lattice in the aliasing model.* There is no compelling evidence in the data for rectangular packing which would have produced only 2 moiré zeroes in 180 degs rather than 3.

The behavior of the moiré zeroes with fringe orientation provides a method to estimate the orientation of the lattice in the living fovea. The orientation at the foveal center was estimated from the phase of the 60 deg harmonic in the data of Figs 8 and 9. It is of some interest to know whether the lattice has the same orientation at the foveal center across individuals, or across eyes within the same individual. The data obtained so far have a tendency to cluster both across and within observers, but an insufficient number of observers have been tested to build a statistical case that it is nonrandom. For example, the probability that the distribution of cardinal axes of all eight eyes determined with the rating technique arose from a random distribution is 11% (Rayleigh test, Batschelet, 1981).

Disorder

The moiré technique for measuring cone spacing described here requires a reasonably regular cone lattice. At retinal eccentricities beyond 1.75 deg, the annulus of zebra stripes cannot be seen at any spatial frequency. Just outside the fovea, observers report the appearance of 2-dimensional spatial noise when viewing fringes above the resolution limit (Williams, 1985a). This noise arises from aliasing by the irregular mosaic of extrafoveal cones, and a

different psychophysical procedure is required to extract estimates of average cone spacing from it (Coletta and Williams, 1987). The degeneration of zebra stripes into spatial noise with increasing eccentricity is consistent with anatomical measurements of disorder in the primate mosaic by Hirsch and Miller (1987). They show that the disorder begins to increase rather abruptly at an eccentricity of about 1–1.5 deg, increasing more slowly at about 2–2.5 deg. It is possible that this disorder reflects the intrusion of rods between the cones.

Even at the foveal center, the data for some of the eyes do not show 60 deg periodicity as clearly as others. For example, the zebra stripe pattern is equally visible in the author's two eyes, but the pattern changes with orientation in a much more regular fashion in the right eye than the left. The reason for this difference probably has more to do with disorder in the foveal lattice than with the insensitivity of the psychophysical techniques. In many instances the irregularities in the data are repeatable from day to day. These deviations probably reveal the presence of permanent faults and distortions in the cone mosaic. The tortuosity of the zebra stripes suggests that the cardinal axes of the triangular array meander across the fovea, and that there is no single set of cardinal axes for the central retina.

Unfortunately, these subjective observations do not lend themselves readily to a quantitative measure of disorder in the lattice. However, they are qualitatively consistent with the disorder seen in all anatomical specimens of the primate fovea (e.g. Borwein *et al.*, 1980; Hirsch and Hylton, 1984; Ahnelt *et al.*, 1987; Hirsch and Miller, 1987). Ahnelt *et al.* (1987) has suggested that disorder often arises because of the presence of a subclass of cone with a larger inner segment. These cones are often surrounded by seven instead of the usual six neighbors. This distortion gives rise to a local change in the orientation of the lattice. Qualitative though they may be, the psychophysical observations have the advantage over anatomical observations that they are not subject to histological insult, confirming that disorder characterizes the intact living fovea.

It is clear that the crystalline triangular lattice described in the foveal aliasing model is appropriate only locally, over distances of perhaps 5–15 min of arc at the foveal center. The simulation in Fig. 7 provides some indication of the "coherence length" of the primate foveal lattice.

*One would predict that the local anisotropy described above would distort the triangular packing of cones so that the angles formed between the neighbors of a given cone would not all equal 60 deg. Unfortunately, the present data do not test this prediction because the local anisotropy is not very large at the foveal center for any of the observers for which the orientation of the lattice was measured.

It diminishes rapidly with increasing eccentricity as rods intrude. Nonetheless, the foveal cone mosaic is sufficiently similar to a regular triangular lattice to allow measurement of the spacing and orientation of the cones in the living human eye.

Acknowledgements—I would like to thank Al Ahumada, Dale Buralli, Mike D'zmura, Nancy Coletta, Kurt Fisher, Joy Hirsch, Ken Knoblauch, Walt Makous, Tim Takahashi, and Bill Vaughn for their contributions to this work. I also thank Joy Hirsch and Bill Miller for supplying photographs of the primate fovea. This work was supported by AFOSR 85-0019, EY04367, EY01319, and EY00269.

REFERENCES

- Ahnelt P. K., Kolb H. and Pflug R. (1987) Identification of a subtype of cone photoreceptor, likely to be blue sensitive, in the human retina. *J. comp. Neurol.* **255**, 18–34.
- Ahuja N. and Schachter B. J. (1983) *Pattern Models*. Wiley, New York.
- Ahumada A. Jr (1986) Models for the arrangement of long and medium wavelength cones in the central fovea. *J. opt. Soc. Am. A* **3**, P92.
- Batschelet E. (1981) *Circular Statistics in Biology*. Academic Press, New York.
- Borwein B., Borwein D., Medeiros J. and McGowan J. W. (1980) The ultrastructure of monkey foveal photoreceptors, with special reference to the structure, shape, size and spacing of foveal cones. *Am. J. Anat.* **159**, 125–146.
- Byram G. M. (1944) The physical and photochemical basis of visual resolving power. Part II. Visual acuity and the photochemistry of the retina. *J. opt. Soc. Am.* **34**, 718–737.
- Campbell F. W. and Green D. G. (1965) Optical and retinal factors affecting visual resolution. *J. Physiol., Lond.* **181**, 576–593.
- Coletta N. J. and Williams D. R. (1987) Psychophysical estimate of extrafoveal cone spacing. *J. opt. Soc. Am. A* **4**, 1503–1513.
- Coxeter H. S. M. (1969) *Introduction to Geometry*, 2nd edn. Wiley, New York.
- Curcio C. A., Sloan K. R. Jr, Packer O., Hendrickson A. E. and Kalina R. E. (1987) Distribution of cones in human and monkey retina: individual variability and radial asymmetry. *Science, N.Y.* **236**, 579–582.
- Drasdo N. and Fowler C. W. (1974) Non-linear projection of the retinal image in a wide-angle schematic eye. *Br. J. Ophthalm.* **58**, 709–714.
- deMonasterio F. M., McCrane E. P., Newlander J. K. and Schein S. J. (1985) Density profile of blue-sensitive cones along the horizontal meridian of macaque retina. *Invest. Ophthalm. visual Sci.* **26**, 289–302.
- Fales C. L., Huck F. O. and Samms R. W. (1984) Imaging system design for improved information capacity. *Appl. Opt.* **23**, 872–888.
- Goodman J. G. (1968) *Introduction to Fourier Optics*. McGraw-Hill, New York.
- Helmholtz H. (1962) *Helmholtz's Treatise on Physiological Optics* (Edited by Southall J. P. C.), 3rd edn. Dover, New York.
- Hendrickson A. E. and Yuodelis C. (1984) The morphological development of the human fovea. *Ophthalmology* **91**, 603–612.
- Hirsch J. and Hylton R. (1984) Quality of the primate photoreceptor lattice and limits of spatial vision. *Vision Res.* **24**, 347–355.
- Hirsch J. and Miller W. H. (1987) Does cone positional disorder limit near-foveal acuity? *J. opt. Soc. Am. A* **2**, 1481–1492.
- Mersereau R. M. (1979) The processing of hexagonally sampled two-dimensional signals. *Proc. IEEE* **67**, 930–949.
- Miller W. H. (1979) Ocular optical filtering. In *Handbook of Sensory Physiology*, Vol. VII/6A. Springer, Berlin.
- Miller W. H. and Bernard G. D. (1983) Averaging over the foveal receptor aperture curtails aliasing. *Vision Res.* **23**, 1365–1369.
- Österberg G. (1935) Topography of the layer of rods and cones in the human retina. *Acta ophthalm., Suppl.* **6**, 1–103.
- Perry V.H. and Cowey A. (1985) The ganglion cell and cone distributions in the monkey's retina: Implications for central magnification factors. *Vision Res.* **25**, 1795–1810.
- Petersen D. P. and Middleton D. (1962) Sampling and reconstruction of wave-number-limited functions in *n*-dimensional euclidean spaces. *Inform. Control* **5**, 279–323.
- Rodieck R. W. (1986) The primate retina. In *Comparative Primate Biology*, Vol IV, *Neurosciences* (Edited by Steklis H. D.). Alan R. Liss, New York.
- Saleh B. E. A. (1982) Optical information processing and the human visual system. In *Applications of Optical Fourier Transforms*, pp. 431–465. Academic Press, New York.
- Smith R. A. and Cass P. F. (1987) Aliasing in the parafovea with incoherent light. *J. opt. Soc. Am. A* **4**, 1530–1534.
- Thibos L. N., Cheney F. E. and Walsh D. J. (1987) Retinal limits to the detection and resolution of gratings. *J. opt. Soc. Am. A* **4**, 1524–1529.
- Williams D. R. (1980) Visual consequences of the foveal pit. *Invest. Ophthalm. visual Sci.* **6**, 653–657.
- Williams D. R. (1985a) Aliasing in human foveal vision. *Vision Res.* **25**, 195–205.
- Williams D. R. (1985b) Visibility of interference fringes near the resolution limit. *J. opt. Soc. Am. A* **2**, 1087–1093.
- Williams D. R. and Coletta N. J. (1987) Cone spacing and the visual resolution limit. *J. opt. Soc. Am. A* **4**, 1514–1523.
- Williams D. R. and Collier R. J. (1983a) Consequences of spatial sampling by a human photoreceptor mosaic. *Science, N.Y.* **221**, 385–387.
- Williams D. R., Collier R. J. and Thompson B. J. (1983a) Spatial resolution of the short-wavelength mechanism. In *Colour Vision: Physiology and Psychophysics* (Edited by Mollon J. D. and Sharpe L. T.), pp. 487–509. Academic Press, New York.
- Wyszecki G. and Stiles W. S. (1982) *Color Science*, 2nd edn. Wiley, New York.
- Yellott J. I. Jr (1982) Spectral analysis of spatial sampling by photoreceptors: topological disorder prevents aliasing. *Vision Res.* **22**, 1205–1210.

APPENDIX

Moiré patterns formed between an interference fringe and a triangular sampling array

This appendix describes the components of the foveal aliasing model in quantitative terms. The effect of the spatial frequency and orientation of an interference fringe on the

spatial frequency of its alias is derived for a perfect triangular array.

Interference fringes. The spatial intensity distribution of an interference fringe, $g(x, y)$, is given by

$$g(x, y) = 1 + \cos 2\pi(v_0x + \omega_0y). \quad (\text{A1})$$

The spatial frequency domain description of the stimulus, $G(v, \omega)$, can be expressed as

$$G(v, \omega) = \delta(v, \omega) + 1/2[\delta(v - v_0, \omega - \omega_0) + \delta(v + v_0, \omega + \omega_0)] \quad (\text{A2})$$

where δ represents the delta function. The distance from the origin of the first-order delta functions specifies the fringe spatial frequency, f , given by

$$f = \sqrt{(v_0^2 + \omega_0^2)}. \quad (\text{A3})$$

The fringe orientation, θ , is given by

$$\theta = \tan^{-1}(\omega_0/v_0). \quad (\text{A4})$$

The lattice of cone centers. The triangular lattice of cone centers, $m(x, y)$ is described by

$$m(x, y) = r^2/\sqrt{3} \sum_{m=-\infty}^{\infty} \sum_{n=-\infty}^{\infty} \times \delta[x - r(m+n), y - r(m-n)/\sqrt{3}]. \quad (\text{A5})$$

For simplicity, we assume an infinite array of receptors with the essential properties of the finite lattice at the foveal center. Its Fourier transform, $M(v, \omega)$, also consists of a triangular lattice of delta functions

$$M(v, \omega) = \sum_{m=-\infty}^{\infty} \sum_{n=-\infty}^{\infty} \times \delta[v - (m+n)/2r, \omega - \sqrt{3}(m-n)/2r]. \quad (\text{A6})$$

Let the Fourier transform of the cone aperture be defined by the function $A(v, \omega)$ whose behavior need not be precisely specified for the moment. The spatial frequency representation of the response of the mosaic, $R(v, \omega)$, when an interference fringe is imaged upon it is

$$R(v, \omega) = G(v, \omega)A(v, \omega)*M(v, \omega) \quad (\text{A7})$$

where * denotes convolution.

Substituting the expressions for $M(v, \omega)$ from equation (A6) and simplifying, we can write

$$\begin{aligned} R(v, \omega) = & \sum_{m=-\infty}^{\infty} \sum_{n=-\infty}^{\infty} \\ & \times \{A(0, 0)[\delta(v - (m+n)/2r, \omega - \sqrt{3}(m-n)/2r)] \\ & + A(v_0, \omega_0)/2[\delta(v - (m+n)/2r - v_0, \omega \\ & - \sqrt{3}(m-n)/2r - \omega_0)] \\ & + A(-v_0, -\omega_0)/2[\delta(v - (m+n)/2r + v_0, \omega \\ & - \sqrt{3}(m-n)/2r + \omega_0)]\} \quad (\text{A8}) \end{aligned}$$

This expression describes the spectrum of an interference fringe of arbitrary spatial frequency and orientation after it has been sampled by a triangular lattice. In addition, the heights of the delta functions in the spectrum have been attenuated by the low pass filtering effects of the cone aperture. That is, the contrast of the alias will be reduced by the cone aperture. Fortunately, the demodulation due to

the cone aperture is not severe enough to obscure the moiré zeroes upon which the psychophysical techniques rest. There is experimental evidence from Byram (1947) and Williams (1985a) that aliasing is visible at frequencies of 150 c/deg or more at the foveal center, which is well above the first harmonic of the foveal cone mosaic (about 112 c/deg). Since the spacing between cones increases faster than the cone aperture with increasing eccentricity, demodulation by the cone aperture is likely to pose an even less severe impediment to the identification of moiré zeroes outside the foveal center.

Let the window of visibility implemented in the model be $W(v, \omega)$. We can define the window as follows:

$$\begin{aligned} & \text{if } |v| + \sqrt{3}|\omega| < 1/r \quad \text{and} \quad |v| < 1/2r, \quad (\text{A9}) \\ & \text{then } W(v, \omega) = 1 \quad \text{otherwise } W(v, \omega) = 0. \end{aligned}$$

To evaluate the output of the model, we need to pass the sampled spectrum described by Equation (8) through the window of visibility. This amounts to retaining all delta functions that fall within the boundaries of the window, and eliminating all others. That is, we multiply the window by the spectral response of the cone mosaic. Let the spatial frequency representation of the output of the model be $O(v, \omega)$. Then

$$O(v, \omega) = R(v, \omega)W(v, \omega). \quad (\text{A10})$$

The preceding description of the model produces an output for any sinusoidal grating of arbitrary spatial frequency and orientation. Below, a more convenient formula is derived for predicting the behavior of moiré patterns for a restricted set of input stimuli that correspond to those used in the psychophysical observations. Consider only those aliases formed by fringes whose first-order spectra lie within a single pair of first-order windows opposite one another with respect to the origin (see Fig. 2). The six-fold rotational symmetry of the mosaic transform and associated windows implies that the behavior of the alias will simply repeat itself for fringe spectra falling within either of the other two pairs of windows. Furthermore, I evaluate the behavior for only one of the two first-order delta functions in the fringe spectrum. The location of only one of these delta functions is sufficient to describe the spatial frequency and orientation of the fringe because of the two-fold rotational symmetry of the fringe spectrum. Thus the problem can be reduced to considering the positions of a delta function within a single first-order window.

Figure 10 shows a portion of the sampled spectrum plotted in Fig. 2. The hexagonal cell on the left corresponds to the zero-order window. The cell on the right corresponds to a single first-order window. Let the coordinates in the frequency plane of the fringe delta function be (v_0, ω_0) . Let the coordinates in the frequency plane of the alias delta function be (v_a, ω_a) . Defining the coordinates of the alias delta function in terms of the coordinates of the fringe delta function, we have

$$v_a = 1/r - v_0 \quad (\text{A11})$$

and

$$\omega_a = -\omega_0. \quad (\text{A12})$$

Thus the moiré frequency, f_a , is given by

$$f_a^2 = [(1/r - v_0)^2 + \omega_0^2]. \quad (\text{A13})$$

Note that this is simply the equation for a circle, whose center has been translated to the coordinates of the center of the first-order window. That is, with the constraint that

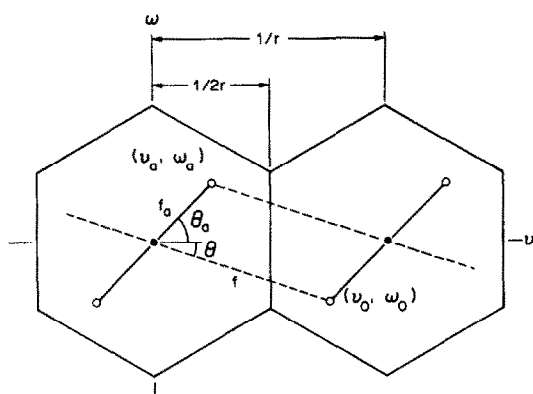


Fig. 10. Diagram of the zero-order window of visibility (left hexagon) and one of the first order windows (right hexagon), illustrating the geometry allowing the spatial frequency of the alias, f_a , to be predicted from the spatial frequency, f , and orientation, θ , of the interference fringe. The fundamental frequency of the mosaic, $1/r$, is shown as is the Nyquist limit from one-dimensional sampling theory, $1/2r$.

the first-order delta function of the fringe spectrum falls within the first-order window, the moiré frequency is determined by the distance of the fringe delta function from the first-order delta function of the mosaic spectrum. Note also that when ω_0 is equal to zero, the expression for the moiré frequency reduces to

$$f_a = 1/r - f_0. \quad (\text{A14})$$

This is the expression for aliasing in one dimension, and yields the familiar Nyquist limit of $1/2r$ when the frequency of the alias, f_a , and the signal, f_0 , are equal.

It is convenient to express equation (13) in terms of the spatial frequency, f , and orientation, θ , of the input fringe instead of the coordinates of one of its first order delta functions in the frequency plane. Thus we have

$$f_a^2 = (1/r - f \cos \theta)^2 + (f \sin \theta)^2. \quad (\text{A15})$$

Recall that this describes the alias spatial frequency for an input frequency whose first-order delta functions fall within a pair of first-order windows opposite each other with respect to the origin. Because there are three such pairs in the frequency plane, the function must repeat itself with an angular periodicity of 60 deg.

Dependence of cone spacing estimate on fringe orientation

Figure 11 shows the dependence of the spatial frequency produced by the model on the spatial frequency of the original interference fringe. The different curves describe the performance of the model for various fringe orientations. A fringe orientation of 0 deg corresponds to the condition where the fringe is parallel to a cardinal axis of the mosaic. In this case the output spatial frequency is proportional to the input spatial frequency up to the Nyquist limit, $1/2r$. At higher spatial frequencies, aliasing appears; the output spatial frequency declines to zero at a spatial frequency of $1/r$, and increases again thereafter. For this particular orientation, a moiré zero can be achieved, and the spatial frequency at which it occurs is the reciprocal of the spacing between rows of cones in the mosaic. At other orientations that do not correspond to cardinal axes, however, the output spatial frequency never reaches zero, although it does pass through a local minimum (indicated by black dots

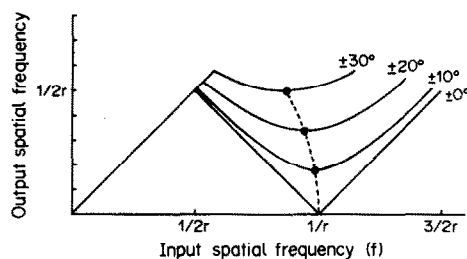


Fig. 11. The output spatial frequency predicted by the model of foveal aliasing as a function of the input spatial frequency of the interference fringe. The parameter for the various curves is the orientation of the input fringe. When the fringe is oriented parallel to a cardinal axis of the mosaic (0 deg curve) a moiré zero occurs for an input frequency of $1/r$. The dotted line indicates how the coarsest moiré pattern shifts slightly toward lower input frequencies with progressive misalignment of the fringe orientation.

in the figure). This local minimum shifts toward lower input frequencies, the larger the mismatch between fringe orientation and a lattice cardinal axis.

The psychophysical measurements of cone spacing were made before the cardinal axes of the mosaic were established, and were therefore not typically made for fringe orientations that corresponded to the cone cardinal axes. The model suggests that, in principle, the technique could overestimate cone spacing when the fringe is not aligned with the cardinal axis of the mosaic. The model predicts that the largest error would be caused by a 30 deg mismatch in fringe orientation and would be about 13%.

The following arguments suggest that in practice this effect is considerably less than 13%. First of all, the average error assuming a random fringe orientation relative to the mosaic, would be less than half the maximum error, or about 5%. Furthermore, the maximum possible mismatch in orientation produces a minimum moiré frequency at very high spatial frequencies, near 60 c/deg at the foveal center. These high spatial frequency aliases would be difficult to see, and probably do not contribute much to the psychophysical judgment. Irregularities in the triangular lattice imply relatively local changes in the lattice orientation. This means that the fringe is likely to be appropriately aligned with the mosaic somewhere within a relatively small retinal region.

An empirical check that fringe orientation did not substantially overestimate cone spacing was made as follows. Two observers (K.K. and D.W.) adjusted the spatial frequency of an interference fringe to minimize the frequency

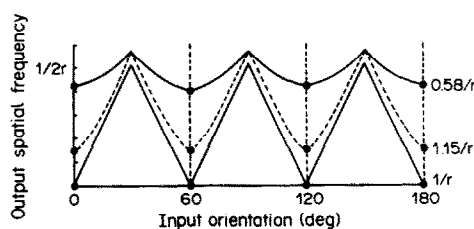


Fig. 12. The output spatial frequency predicted by the model of foveal aliasing as a function of the input orientation of the interference fringe. The parameter for different curves is the input fringe spatial frequency. When the fringe equals the fundamental frequency of the mosaic, $1/r$, moiré zeroes occur every 60 deg, whenever the fringe becomes aligned with the rows of cones in the triangular lattice.

of the alias at the foveal center when the fringe was oriented along each of the three cardinal axes, and when it was oriented between each of the three axes. The mean estimate of cone spacing was 4.8% less in the off-axis than the on-axis condition, which is the expected direction. However, the two conditions were not significantly different (two-tailed t -test, $\alpha = 0.10$).

Dependence of lattice orientation estimate on fringe spatial frequency

Figure 12 shows how the output spatial frequency of the model depends on the orientation of the input fringe, where the spatial frequency of the input fringe is a parameter for the different curves. If input spatial frequencies below the Nyquist frequency had been plotted, they would appear as

horizontal lines in this plot, since they would be accurately reconstructed by the model. All the curves are for input spatial frequencies that are undersampled by the triangular lattice, show that the behavior of the moiré patterns can be seen. In each case, the output spatial frequency oscillates as a function of input fringe orientation, with a period of 60 deg. This periodicity has the largest amplitude when the fringe spatial frequency equals the reciprocal of the spacing between rows in the mosaic. In this particular case, the moiré pattern reaches zero spatial frequency, creating a moiré zero every 60 deg. These predictions would resemble a 6 pointed starfish if plotted in polar coordinates. Errors in the estimate of row spacing have no effect on the estimate of the orientation of the lattice since the orientation producing the minimum output frequency always corresponds to a cardinal axis.